**Letter** **Open Access**

Diego Pallarola[a], Ilia Platzman[a], Alexander Bochen, Elisabetta A. Cavalcanti-Adam, Markus Axmann, Horst Kessler, Benjamin Geiger and Joachim P. Spatz*

# Focal adhesion stabilization by enhanced integrin-*c*RGD binding affinity

DOI 10.1515/bnm-2016-0014
Received October 24, 2016; accepted January 19, 2017; previously published online February 23, 2017

**Abstract:** In this study we investigate the impact of ligand presentation by various molecular spacers on integrin-based focal adhesion formation. Gold nanoparticles (AuNPs) arranged in hexagonal patterns were biofunctionalized with the same ligand head group, cyclic Arg-Gly-Asp [*c*(-RGDfX-)], but with different molecular spacers, each of which couples the head group to the gold. Aminohexanoic acid, polyethylene glycol (PEG) and polyproline spacers were used to vary the distance between the binding motif and the substrate, and thus the presentation of integrin binding on anchoring points. Adherent cells plated on nanopatterned surfaces with polyproline spacers for peptide immobilization could tolerate larger ligand spacing (162 nm) for focal adhesion formation, in comparison to cells on surfaces with PEG (110 nm) or aminohexanoic acid (62 nm) spacers. Due to the rigidity of the polyproline spacer, enhanced access to the ligand-binding site upon integrin-*c*RGD complex formation increases the probability of rebinding and decreases unbinding, as measured by fluorescence recovery after photobleaching (FRAP) analysis, compared to the analogues with aminohexanoic acid or PEG-containing spacers. These findings indicate that focal adhesion formation may not only be stabilized upon tight integrin clustering, but also by tuning the efficiency of the exposure of the *c*RGD-based ligand to the integrin extracellular domains. Our studies clearly highlight the importance of ligand spatial presentation for regulating adhesion-dependent cell behavior, and provide a sound approach for studying cell signaling processes on nanometer-scale, engineered bioactive surfaces under chemical stimuli of varying intensities.

**Keywords:** biointerfaces; cell adhesion; cyclic RGD; integrins; ligand binding affinity; polyproline spacer.

## Introduction

Integrin-mediated cell adhesion to the extracellular matrix (ECM) is crucial for multiple cellular functions such as cell proliferation, survival, migration and differentiation and has been extensively studied, both in vivo and in vitro [1]. Integrins are a diverse family of heterodimeric ECM receptors [2, 3], consisting of α- and β-subunits, that span the plasma membrane, and connect the actin cytoskeleton to specific peptide motifs such as Arg-Gly-Asp (RGD) within the ECM. Conformational rearrangement of the integrin dimers from an inactive to an active state enables cells to achieve a high-affinity state and interact with the ECM ligands [4, 5]. Further recruitment of different anchoring and adapter proteins [6, 7] promotes the clustering of activated integrins, leading to the assembly of three-dimensional cross-linked structures known as focal adhesions (FAs) [8]. Fundamental structural and functional characterization of these complex cell-ECM adhesion sites is a compelling goal, mainly due to the molecular and architectural complexity of the ECM and the corresponding processes [1].

[a]**Diego Pallarola and Ilia Platzman:** These authors contributed equally to this study.
***Corresponding author: Joachim P. Spatz,** Department of Cellular Biophysics, Max-Planck-Institute for Medical Research, Jahnstr. 27, 69120 Heidelberg, Germany; and Department of Biophysical Chemistry, Institute of Physical Chemistry, Heidelberg University, 69120 Heidelberg, Germany, Phone: +49 711 689 3610, Fax: +49 711 689 3612, E-mail: Spatz@is.mpg.de
**Diego Pallarola:** Instituto de Nanosistemas, Universidad Nacional de General San Martín, Av. 25 de Mayo y Francia, San Martín, 1650, Argentina
**Ilia Platzman, Elisabetta A. Cavalcanti-Adam and Markus Axmann:** Department of Cellular Biophysics, Max-Planck-Institute for Medical Research, Heisenbergstr. 3, 70569 Stuttgart, Germany; and Department of Biophysical Chemistry, Institute of Physical Chemistry, Heidelberg University, 69120 Heidelberg, Germany
**Alexander Bochen and Horst Kessler:** Department of Chemistry, Institute for Advanced Study and Center for Integrated Protein Science, Technische Universität München, Lichtenbergstr. 4, 85747 Garching, Germany
**Benjamin Geiger:** Department of Molecular Cell Biology, The Weizmann Institute of Science, 7610001 Rehovot, Israel

In recent years, novel strategies were developed, based on the engineering of biomimetic matrices for controlled stimulation of cells in vitro, particularly in key biomedical applications such as stimulation of immune cells, controlling pluripotency and regulating cell migration [9, 10]. The use of such surfaces enabled testing the effects of ECM ligands diversity, as well as the effects of integrin receptor occupancy and clustering [11]. Early studies focused on the process of integrin aggregation and FA formation in different ECM environments in vitro [12, 13]. It was shown that by controlling cluster size, affinity, and average ligand density and spacing, cell migration and spreading behaviors, as well as FA assembly and maturation could be affected. Supported by theoretical modeling [14], these studies suggested that by increasing receptor-ligand interactions, and thus the amount of occupied receptors, clustered ligands enhanced binding affinity and, concomitantly, adhesion strength. Nevertheless, these approaches suffered from variations in ligand distribution due to random ligand grafting. Recent progress in surface patterning techniques made it possible to control the precise placement of individual anchoring ligands at nanoscale resolution [15–17]. These studies indicated that integrin binding and clustering, the consequent assembly of FAs and cell spreading are strongly influenced by fine changes in adhesive cues. It has been proposed that inter-ligand spacing ranging from 58 to 73 nm is required for successful integrin-mediated signaling activation [15, 16], and that local, more than global ligand distribution seems to be a key surface parameter for the assembly and stability of FA complexes [18–20]. At the nanoscale, the number and geometric distribution of receptors, as well as their binding strengths, exert a profound effect on cell adhesion strength, by means of a cooperative integrin clustering mechanism [20–22]. Although the physiological relevance of ligand spacing regulation is still unclear, these findings clearly expose the exquisite cellular sensing machinery, thus providing a sound approach for further eliciting and unraveling specific cellular responses to their environment.

Among the peptides known to support cell adhesion, the tri-amino acid sequence RGD is the most widely studied [23–25]. This sequence is ubiquitously expressed in many ECM components [3, 26], and serves as a minimal essential binding motif for several different integrins [25], although it binds primarily to the integrin subtype αvβ3 [27]. Cyclization [28], which confers structural rigidity and thus chemical stability, and other non-natural peptide modifications such as D-amino acid incorporation [29] and N-methylation [30, 31], are commonly employed to improve the selectivity and affinity of the RGD sequence for a specific integrin subtype [32]. Apart from strategies for restricting the conformational space of a ligand, multivalency can further enhance its affinity for target cells by displaying additional epitopes able to promote rebinding [33–35]. Notably, a minimum distance between the RGD peptides and the anchoring substrate is required, such that the binding motifs are adequately oriented to facilitate integrin binding [36, 37]. Aliphatic [38, 39] and polyethylene glycol [40, 41] (PEG)-based short polymers, as well as amino acid chains [42, 43] (e.g. polyglycine, polyproline) have been used as spacers for peptide immobilization. Nonetheless, despite their wide use, ligands bearing aliphatic and PEG spacers may experience a decrease in binding affinity [10, 44]. Densely packed monolayers and spacer flexibility may prevent optimal exposure of the integrin ligands. Recently, we compared the influence of different spacer systems, namely alkane-, PEG-, and polyproline-based sequences, on the affinity of a *c*(-RGDfX-)-containing ligand to αvβ3 integrin [43]. Our findings demonstrated that the more extended nature of the polyproline spacers and the low-density assemblies they yield, the more precisely and constructively ligand display could be controlled, thus enhancing *c*RGD-integrin interactions at the adhesion sites.

In the present work, we aim to provide insights into the role of ligand binding and integrin adhesion ligand clustering in regulating cell adhesive responses, by comparing cell behavior on substrates that present *c*(-RGDfX-)-containing ligands of different binding affinities to its primary target, αvβ3 integrin. Ligands were precisely positioned at different lateral distances by means of a gold nanoparticle (AuNP) pattern, enabling for variations in the density of anchor binding points at the nanoscale. Interactions between the integrin extracellular domains and the *c*(-RGDfX-)-binding domains were evaluated in response to variations in ligand presentation, by means of different spacer systems.

## Results and discussion

Our approach to engineer cellular environments with the ability to enable specific cell-*c*RGD interactions at precisely localized positions on a non-adhesive PEG-background was based on a previously established technique, namely diblock-copolymer micelle nanolithography (BCML) [45]. In detail, glass coverslips were patterned with AuNPs of 6 and 9 nm diameter arranged in a quasi-hexagonal structure, with an average interparticle distance varying from 62 to 162 nm. The glass surface between the AuNPs was

then passivated with PEG-terminated siloxane [46], to render a biologically inert background that does not initiate any cell activation. This approach is very powerful, since it allows for variations in both the average surface density, and the local spatial distribution of ligands in well-defined nanoscopic geometries. Subsequently, AuNPs were functionalized with different *c*RGD-based thiol ligands. The *c*RGD-based pentapeptides selected for this study exhibit different integrin αvβ3 binding affinities, as tested in a soluble adhesion-inhibition assay (Table 1). As shown in Figure 1, each ligand consists of three main elements: (i) a monomeric or dimeric integrin-binding group; (ii) a spacer molecule; and (iii) a thiol-based anchoring group. Compounds **1** and **2** bear a flexible spacer such as an aminohexanoic acid (Ahx) or a PEG-based spacer, respectively, while compound **3** consists of a *c*(-RGDfE-) dimer ligated to a more rigid polyproline sequence. The influence of spacer type and length has a remarkable effect on the overall binding affinity towards αvβ3 integrin [43], making these compounds excellent candidates for studying the cellular response to chemical signaling of varying affinities within its environment.

**Table 1:** Inhibition of αvβ3 integrin binding to vitronectin by *c*RGD pentapeptides.

| Peptide description | $IC_{50}$[a] αvβ3, nM |
|---|---|
| **1** *c*(-RGDfK[Ahx-MPA]-) | 15.7 ± 4.5 |
| **2** *c*(-RGDfK[Hegas-(cta)$_3$]-) | 19.5 ± 2.9 |
| **3** [*c*(-RGDfE[HexPPPPPP]-)]$_2$K-cta | 0.17 ± 2.4 |
| *c*(-RGDfK-)[b] | 2.6 ± 0.6 |
| Cilengitide[c] | 0.54 ± 0.02 |

[a]$IC_{50}$ values were obtained from a competitive ELISA using the natural ligand, vitronectin (Vn), and the soluble integrin αvβ3 [43].
[b]This cyclic pentapeptide was used as precursor for the design of **1**–**3**, and as a competitive agent in αvβ3 integrin binding assays.
[c]Cilengitide, *c*(-RGDf$^{Me}$V-) [30], was used as an internal reference compound for the integrin αvβ3 ELISA assay.
Ahx, 6-amino-hexanoic acid; cta, cystamine; Hegas, heptaethylene glycol amino acid (PEG thiol acid); Hex, 4-(1-(2-aminoethyl)-1*H*-1,2,3-triazol-4-yl)butanoic acid; MPA, mercaptopropionic acid.

In the following, the impact of (i) three chemically different ligands, (ii) ligand density (i.e. the distance between gold dots) and (iii) particle size, on the integrin-mediated cell adhesion were examined. Rat embryonic fibroblasts [REF52 wild-type (WT) cells] were seeded on the individual *c*RGD-functionalized adhesive surfaces for 4 h, and then visualized by phase contrast microscopy (Figure 2). It is evident that fibroblasts spread on the 62 nm patterns,

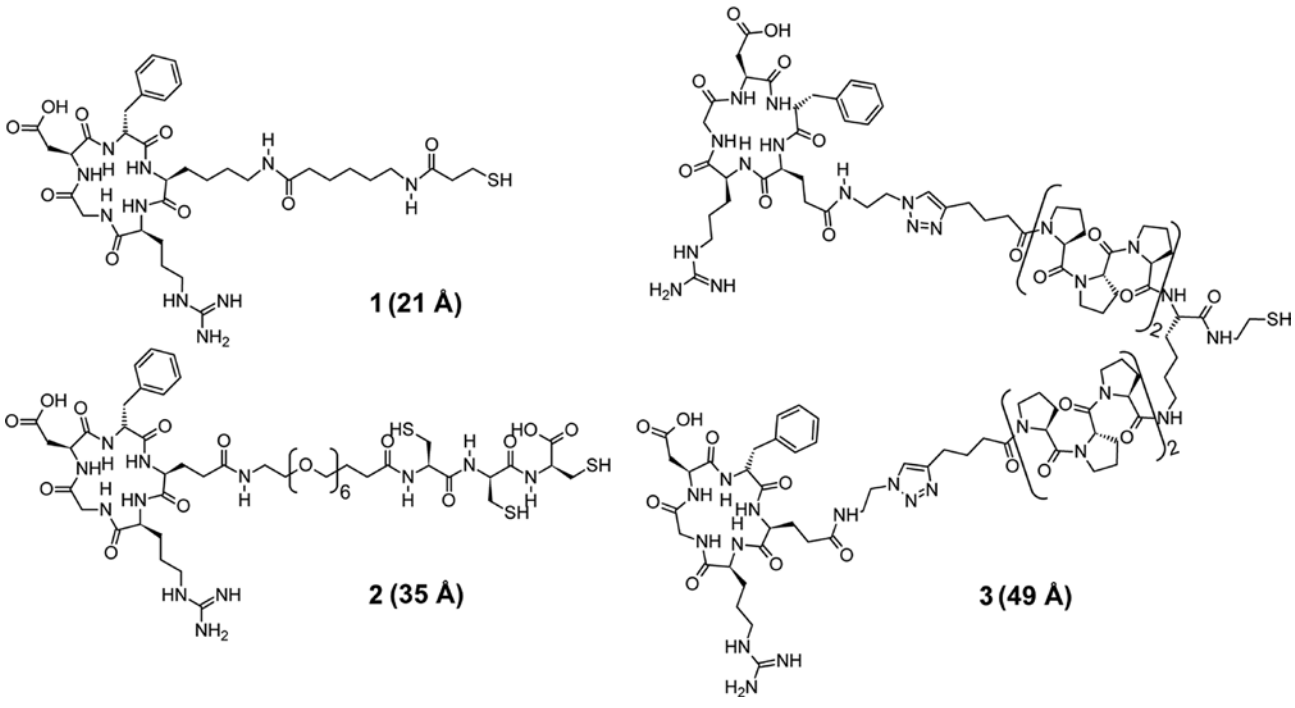


**Figure 1:** Molecular structure of the peptides examined in this study. **1** and **2**) Ligand peptide composed of a *c*RGD headgroup with an aminohexanoic acid (Ahx) (**1**), or a polyethylene glycol (PEG)-type spacer (**2**). **3**) Ligand peptide consisting of a *c*RGD headgroup dimer ligated to a polyproline spacer.
Spacer length in brackets was calculated for the all-*trans* configuration of aliphatic and PEG spacers between Cα Lys(K) and thiol, and for proline spacers between Cα Glu(E) and thiol. All compounds have a thiol system for surface attachment (gold-SH bond).

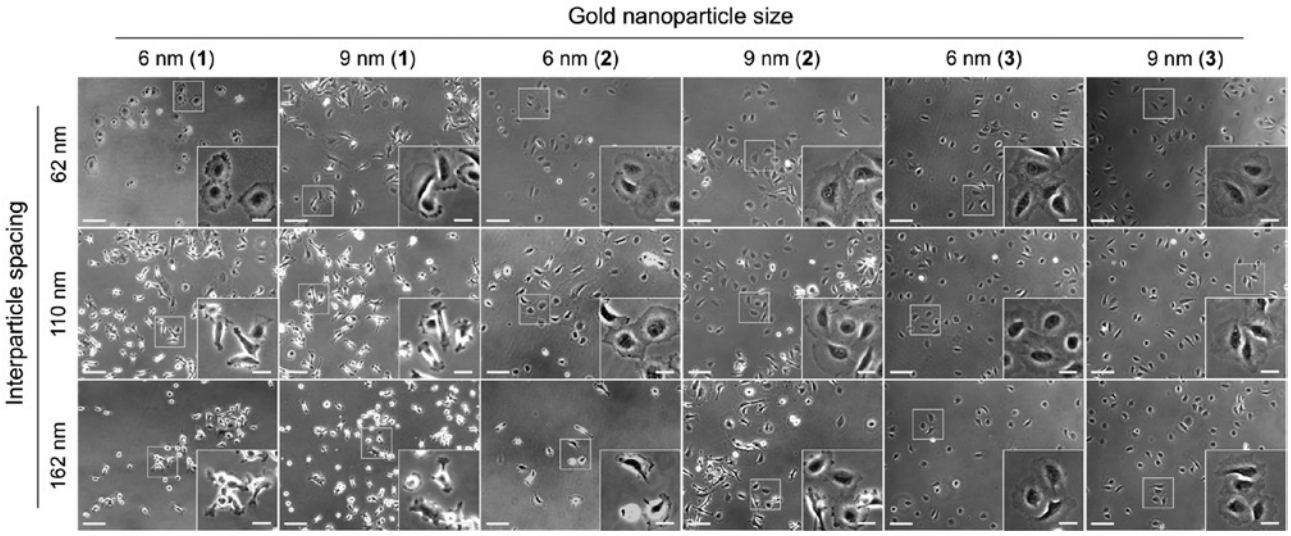


**Figure 2:** Phase contrast images of REF52 WT cells 4 h after seeding on nanostructured glass surfaces functionalized with compound **1** (*c*(-RGDfK[Ahx-MPA]-), **2** (*c*(-RGDfK[Hegas-(cta)$_3$]-), and **3** ([*c*(-RGDfE[HexPPPPPP]-)]$_2$K-cta) with varying particle sizes (6–9 nm) and interparticle distances (62–162 nm).
Scale bar: 100 μm. Insets: Magnification of the selected areas. Scale bar: 30 μm.

as indicated by their typical morphology. However, distinct differences in adhesion-based cell responses are noticeable between the ligands on substrates with 110 and 162 nm interparticle distances. Ahx-based ligand led to limited cell spreading, characterized by elongated cellular morphology. This effect was even more pronounced on substrates with 162 nm-spaced AuNPs, where more elongated cell spreading and an increased number of quiescent cells could be observed. Conversely, 62 and 110 nm patterns functionalized with the PEG-based ligand were sufficient to support spreading via αvβ3 integrin-*c*RGD interactions, while cells plated on 162 nm patterns exhibit a behavior similar to that observed on 110 nm patterns functionalized with the Ahx-based ligand.

Cell behavior on AuNPs-structured surfaces functionalized with the polyproline-based ligand is remarkable. Well-spread cells with a radial morphology can be observed, regardless of the distance between AuNPs. Similar results were obtained with mouse calvaria osteoblasts (MC3T3 cells), indicating a more generalized cell adhesion behavior (Figure S3). These findings suggest that the divalent polyproline-based ligand provides superior binding affinity to αvβ3 integrin, thus supporting cell adhesion and spreading even at very low ligand densities. These observations are quantitatively summarized through the projected cell area analysis as depicted in Figure 3. Furthermore, we characterized the cellular response on gold nanopatterns functionalized with the polyproline-based ligand at larger interparticle distances (162–280 nm), showing that limited cell adhesion takes

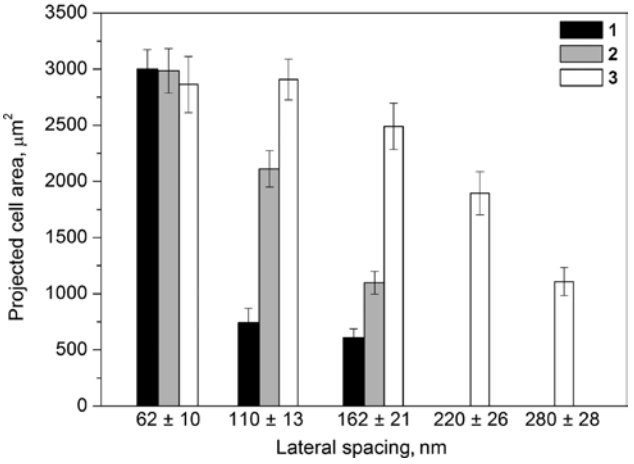


**Figure 3:** Projected cell area analysis of REF52 WT cells 4 h after seeding on 9 nm AuNP-patterned glass surfaces functionalized with the different *c*RGD pentapeptides.
Data are presented as mean ± s.e.m., n > 50, p < 0.01.
**1**: *c*(-RGDfK[Ahx-MPA]-) (black); **2**: *c*(-RGDfK[Hegas-(cta)$_3$]-) (gray); **3**: [*c*(-RGDfE[HexPPPPPP]-)]$_2$K-cta (white).

place when the particle spacing is increased above 220 nm (Figure 3). This critical interparticle distance is more than three times the value previously reported [15], and verified in this work, for the Ahx-based ligand, highlighting the critical influence of the ligand-binding affinity at the integrin-adhesion site.

To determine whether the observed cell behavior is purely controlled by the chemical features of the ligand-presenting molecules or is also influenced by the

dimensions of the binding domains, we varied the AuNP size from 6 to 9 nm, to measure the sensitivity of the adherent tissue cells to variations in the presentation of adhesive ligands at the anchoring points. In the case of the Ahx- and PEG-based ligands, changes in cell adhesive response are barely noticeable if the size of AuNPs is increased: a slight reduction in the number of quiescent cells and a discrete widening of the lamellipodia is seen in 110 nm patterns functionalized with the alkane-based compound, and 162 nm patterns functionalized with the PEG-based compound, compared with the analogous 6 nm AuNP patterns. Cells seeded on gold patterned substrates bearing the polyproline-based ligand showed no visible dependence on particle size within the evaluated regime. We can thus infer that variation in cell-substratum adhesion interaction is mainly governed by the spatial organization and the chemical features of the *c*RGD-based ligands. These observations also suggest that more than one integrin dimer interacting with one single domain is an unlikely scenario. Considering that the diameter of an integrin dimer varies between 8 and 12 nm [47], it is reasonable to assume that each *c*RGD-coated AuNP provides an individual binding site, due to steric hindrance. Thus, potential multiple integrin binding does not account for cell adhesion-associated responses on 9 nm AuNP nanoarrays. Moreover, the height of the nanoparticles was adjusted to at least the height of the PEG layer (~6 nm), resulting in adequate exposure of the integrin-binding group. Nevertheless, topographical effects [48–52] and the promotion of integrin rebinding [53–56] due to increase in particle size and ligand population cannot be ruled out. However, the observed phenomena could be explained in terms of the availability of the *c*RGD head group for binding, as well as its ability to promote ligand rebinding. These two features are mainly attributed to the chemical nature of the ligand-presenting molecule, and will be discussed in further detail later [43]. Notably, cells in control experiments performed on PEG-passivated surfaces lacking AuNPs and/or *c*RGD functionalization did not adhere to the substrates. Furthermore, X-ray photoelectron spectroscopy of non-patterned substrates incubated with the different *c*RGD pentapeptides showed no evidence of ligand intercalation within the PEG brush layer (data not shown). This confirms that cell adhesion responses as reported herein are entirely due to the activation of αvβ3 integrin, through its interaction with *c*RGD-functionalized AuNPs.

A hallmark of integrin-mediated cell adhesion is the formation of FAs and the assembly actin stress fibers [1, 57]. To address whether those tailored surfaces activate integrin signaling, we compared the influence of the three different ligands on the assembly of FAs and actin fibers. REF52 WT cells were plated for 4 h on nanopatterned surfaces with different inter-ligand spacings, then fixed and stained for paxillin, zyxin and actin. Paxillin resides in both initial adhesion contacts [58]; namely, focal complexes (FXs), and mature adhesions, while zyxin is recruited during the maturation of these FXs into FAs, and constitutes a distinctive protein of mature FAs [59]. Examination of the labeled cells revealed extensive cell adhesion and spreading on the 62 nm *c*RGD-nanopatterns, indicating successful integrin-ligand interactions with all the different compounds (Figure 4, first column). Similar paxillin- and zyxin-rich FA distribution was observed for the different compounds, as well as actin fibers organized as a dense meshwork of peripheral actin filaments, although with a higher density of stress fibers in the case of the polyproline-based compound (Figure S4). In agreement with Figure 2, cells growing on 110 nm patterns exhibited distinctive features (Figure 4, second column). On substrates functionalized with the Ahx-based ligand, cells were considerably less spread than those plated on the 62 nm nanopatterns, and failed to develop FAs and to induce stress fiber assembly. In contrast, cells plated on 110 nm patterns functionalized with the PEG- or polyproline-based ligand showed stable integrin-mediated adhesion characterized by radial spreading, and co-localized paxillin and zyxin patches mainly distributed at the periphery of the cells (Figure S4). The effect of *c*RGD peptide spacing on the cellular response was even greater when AuNPs were separated by 162 nm (Figure 4, third column). Cells plated on substrates coated with the alkane-based compound showed very poor adhesion and spreading, resulting in complete removal of cells after gentle rinsing. Cell behavior observed on nanopatterns functionalized with the PEG-based ligand is consistent with a spreading and motility regime characterized by repeated extension-retraction cycles [16]. Such cells became highly polarized, displaying small paxillin and zyxin clusters at low density, restricted to the cell edges (Figure S4). Conversely, the polyproline-based compound is able to circumvent these limitations, providing a suitable environment for the cells to attach and spread. These substrates supported good cell adhesion with well-constituted paxillin- and zyxin-rich adhesions, as well as organized actin fibers (Figure S4), similar to what was observed on dense nanopatterns.

Ligand binding to integrins induces conformational reorganization of the α and β-integrin dimer, leading to integrin activation and clustering, and the subsequent signal propagation that leads to events such as cell adhesion and proliferation [60]. This highly regulated process

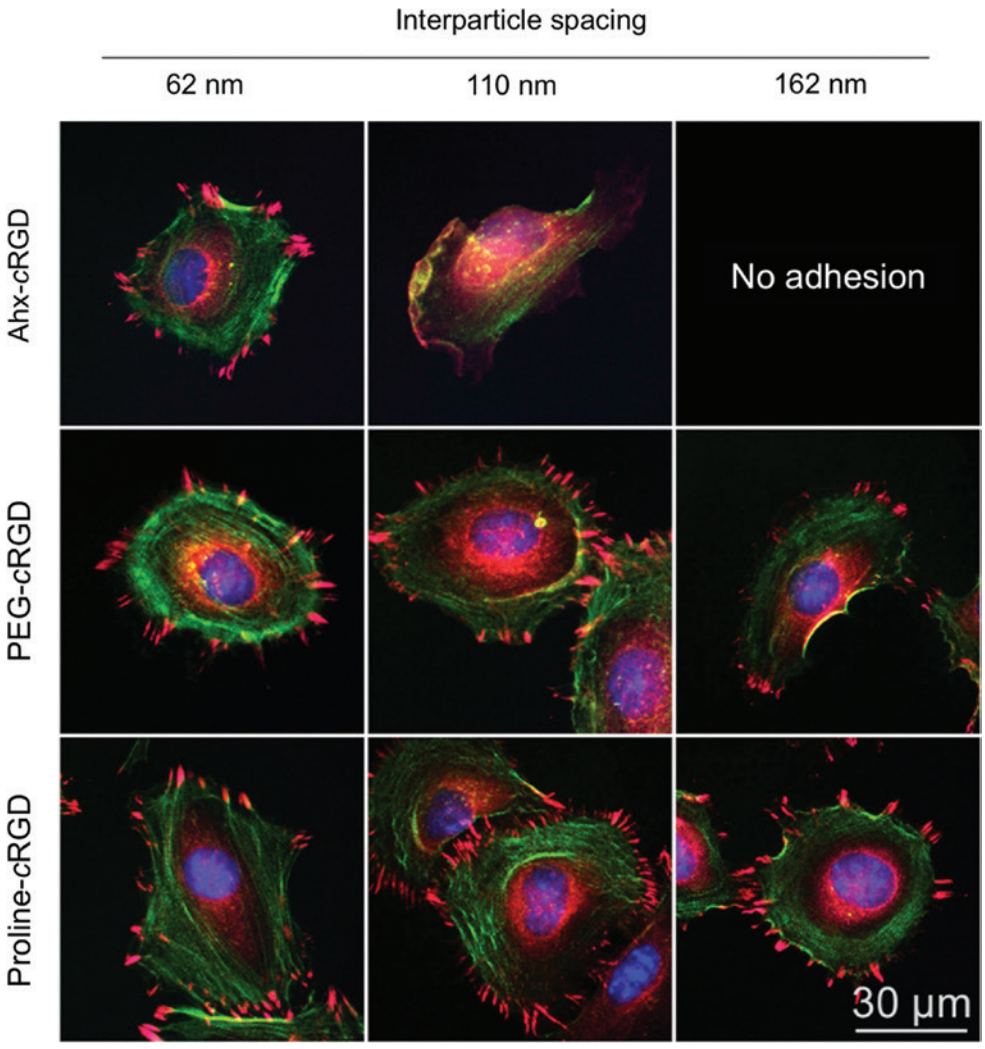


**Figure 4:** Fluorescent micrographs of representative REF52 WT cells on nanopatterns with different interparticle distances, and functionalized with *c*(-RGDfK[Ahx-MPA]-, *c*(-RGDfK[Hegas-(cta)$_3$]-, and [*c*(-RGDfE[HexPPPPPP]-)]$_2$K-cta.
Following 4 h of incubation, cells were fixed and stained for paxillin (red), zyxin (pink), actin (green) and nuclei (blue).

is essential for initiation of FAs, which are tightly associated with the cytoskeletal network, enabling cells to respond to diverse physical and chemical environmental signals [1]. As integrin epitope activity promotes the formation of stable integrin-*c*RGD complexes, it is also likely that high-affinity interactions between the receptors and binding sites may promote enhancement of specific cellular responses. An example of this finely-tuned crosstalk between FAs and actin filaments is the appearance of high-frequency FA nucleation in cells adhering to high-affinity substrates [61, 62]. Minimal requirements for cell adhesion were also found to be sensitively dependent of ligand affinity. WT NR6 fibroblasts seeded on substrates grafted with star-shaped PEG macromolecules functionalized with YGRGD peptide exhibited a substantially lower threshold spacing for FA and stress fiber development [13], compared with similar studies performed with human foreskin fibroblasts on the randomly immobilized ligand GRGDY, in which case a minimal peptide-to-peptide spacing of 140 nm was required for FA and stress fiber formation [12]. This difference was mainly attributed to the much lower affinity of the YGRGD ligand compared to the GRGDY ligand, which implies that a much higher ligand density would be required for YGRGD to obtain equivalent values of receptor occupancy. Although both approaches lack a spatial distribution of ligands that is precisely localized and predefined, these studies provide compelling evidence for the importance of integrin-ECM binding affinity in stimulating adhesion-mediated signaling.

In order to shed light on the role of biomimetic surface properties in regulating adhesive interactions, we investigated the effects of the different *c*RGD ligands on the

binding of αvβ3 integrin. Two different in vitro binding assays were conducted, to determine: a) the binding affinity of αvβ3 integrin, and b) the dissociation rate of αvβ3 integrin-*c*RGD complexes. The binding affinity of αvβ3 integrin towards *c*RGD nanopatterns was evaluated as the median inhibitory concentration ($IC_{50}$) in a competitive ELISA. *c*RGD-functionalized nanopatterns with a 62 nm interparticle distance and 9 nm particle size, soluble αvβ3 integrin, and soluble *c*(-RGDfK-) as a competitive binding reagent were used. Dose-response curves for the binding of αvβ3 integrin in the presence of different concentrations of *c*(-RGDfK-) to nanopatterns coated with either the PEG- or the polyproline-based ligand are shown in Figure 5A and B, respectively. Data from these assays were fit to a 4-parameter logistic model; the derived binding affinities are summarized in Table 2. Consistent with the results of the previously described cell adhesion experiments, the polyproline-based ligand displayed a higher affinity for αvβ3 integrin binding than the analogue bearing a PEG-based spacer (i.e. $IC_{50}$**3** > $IC_{50}$**2**). Data for the alkane-based ligand could not be evaluated, due to the low fluorescence intensity measured under the experimental conditions (Figure S5). The efficacy of the polyproline-based spacer as a ligand-presenting molecule is

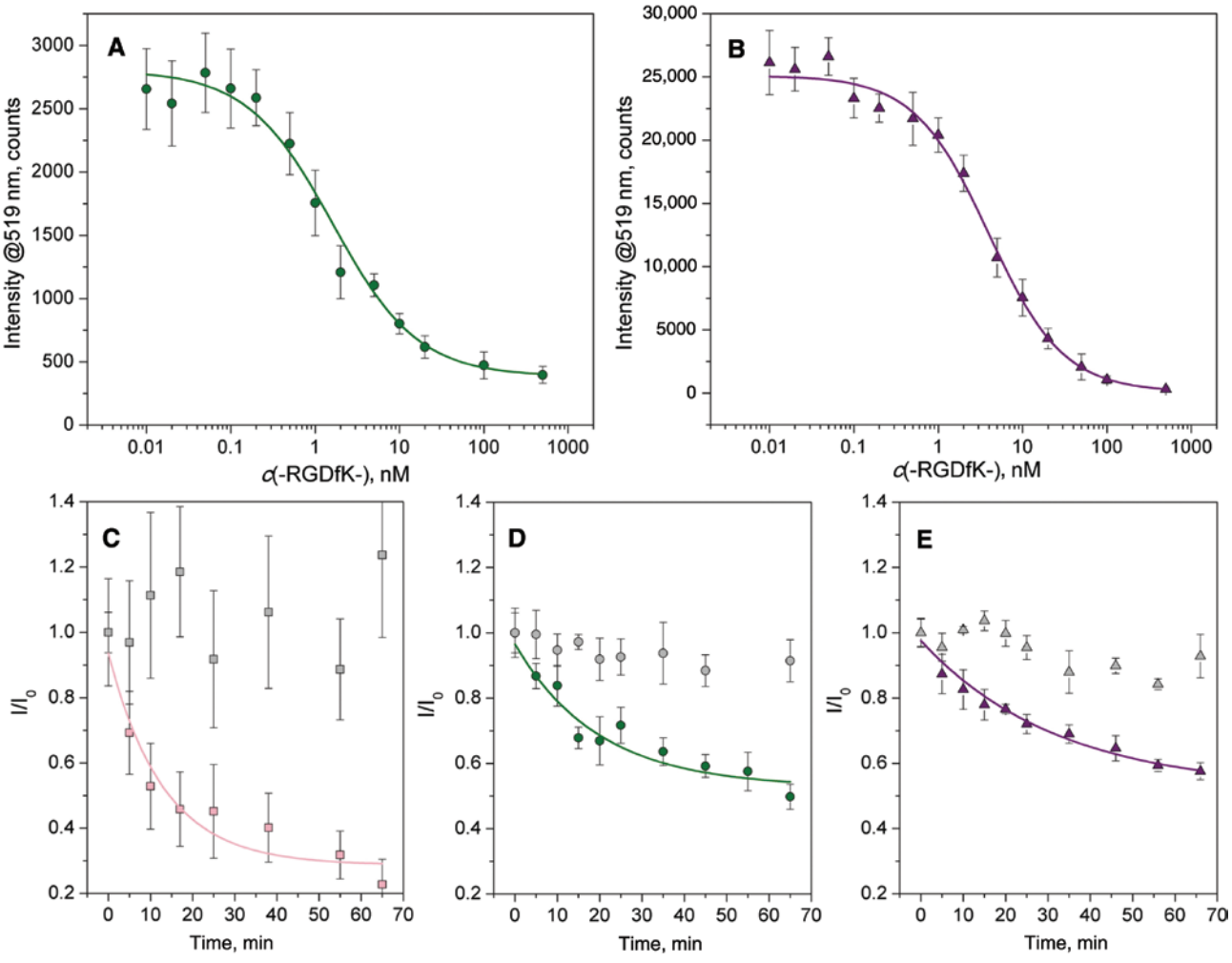


**Figure 5:** (A and B) Inhibition of αvβ3 integrin binding to nanopatterns functionalized with compound **2** (*c*(-RGDfK[Hegas-(cta)$_3$]-), and **3** ([*c*(-RGDfE[HexPPPPPP]-)]$_2$K-cta) by the soluble pentapeptide *c*(-RGDfK-).
Inhibition data at each concentration of *c*(-RGDfK-) are an average of three independent experiments ± standard deviation. The dose-response data are fit to a 4-parameter logistics model. (C–E) Effect of the soluble pentapeptide *c*(-RGDfK-) (100 μM) on αvβ3-*c*RGD complex dissociation on nanopatterns functionalized with compound **1** (*c*(-RGDfK[Ahx-MPA]-) (C), **2** (*c*(-RGDfK[Hegas-(cta)$_3$]-) (D), and **3** ([*c*(-RGDfE[HexPPPPPP]-)]$_2$K-cta) (E). The data are fit to a first-order kinetic equation to obtain the dissociation rate constants ($k_{diss}$) and half-lives ($t_{1/2}$) of the αvβ3-ligand complex. Data at each time point are presented as an average of three independent experiments ± standard deviation. Each plot (C–E) includes the data (gray symbol) corresponding to the αvβ3-*c*RGD complex dissociation kinetics, in the absence of *c*(-RGDfK-).

**Table 2:** Characterization of αvβ3 integrin binding to *c*RGD-functionalized nanopatterns.

| Peptide | $IC_{50}$[a] αvβ3, nM | $k_{diss}$[b], $10^3$ $min^{-1}$ | $t_{1/2}$[b], min |
|---|---|---|---|
| **1** | n.d.[c] | 17.92 ± 7.90 | 38.7 ± 17.0 |
| **2** | 1.5 ± 0.7 | 9.03 ± 2.41 | 76.7 ± 20.4 |
| **3** | 3.3 ± 0.6 | 7.53 ± 1.64 | 92.0 ± 20.1 |

[a]$IC_{50}$ values were obtained by fitting the competition binding curves (Figure 5A and B) according to a 4-parameter logistics model.
[b]Kinetics parameters $k_{diss}$ and $t_{1/2}$, were extracted by fitting the dissociation curves (Figure 5C–E) to a first-order kinetic equation.
[c]Experimental conditions were such that the intensity of the fluorescence signal was very low, making the analysis unviable.

reflected by the amplitude of the response plotted on the Y-axis. The fluorescence intensity value obtained for nanopatterns coated with this ligand in the absence of competition is almost 10-fold higher than that seen with the PEG-based ligand (Figure S5). It is also worth mentioning that at higher concentrations of *c*(-RGDfK-), both curves reach similar low values, indicating negligible, unspecific binding of αvβ3 integrin to the substrates. Moreover, no binding inhibition was observed when a highly selective α5β1-antagonist, c(-*phg*-isoDGRk-) [63], was used, even at a concentration of 500 nM, demonstrating the specificity of the integrin binding process.

Dynamic monitoring of fluorescently labeled αvβ3 integrin was carried out to assess and compare the dissociation rate of the αvβ3 integrin-*c*RGD complexes prepared in vitro, as described in the Methods section. The integrin-specific association with the *c*RGD-particle adducts was conducted in the absence of competitive ligands over a 24 h period. Surfaces were then rinsed to remove loosely bound integrins, and incubated with 100 μM *c*(-RGDfK-). The corresponding dissociation curves for the different *c*RGD-coated nanopatterns are shown in Figure 5C–E. Dissociation data were fit to a simple exponential decay curve to extract the dissociation constants ($k_{diss}$) and half-life ($t_{1/2}$) of the αvβ3 integrin-*c*RGD complexes, as presented in Table 2. The results clearly show the reversible nature of the interaction between αvβ3 integrin and the *c*RGD head group; furthermore, disruption of this interaction is highly dependent on the ligand-presenting molecule. The αvβ3 integrin-*c*RGD complex dissociates rapidly from nanopatterns functionalized with the Ahx-based ligand, at a rate that is 2- to 3-fold greater than the analogues with the PEG- and polyproline-based ligands, respectively.

Once established, the inherent stability of the αvβ3 integrin-*c*RGD complex is equivalent for the different ligands, since the pharmacophoric molecule remains the same. Therefore, the variations in dissociation rates obtained for the different substrates can be ascribed to the accessibility of the binding complex, and to the ability of the ligand to promote rebinding upon complex dissociation. These opposite effects are intimately linked to ligand density and orientation at the binding nanodomains (i.e. AuNPs). High accessibility to the ligand-binding pocket increases both the association and dissociation rates of the integrin-ligand complex and, at the same time, provides a favorable scenario for ligand rebinding, thereby contributing to the stability of the complex [55]. Several studies conducted on the recognition-driven assembly of proteins showed that the binding accessibility of a protein is decreased in densely packed assemblies of the target molecule, compared to those with lower molecule density [13, 37, 64, 65], a finding mainly attributed to steric inhibition of the binding. Orientation and presentation of the binding domain very much depends on the nature of the spacer.

Conformational changes caused by a flexible and/or too long spacer can result in the shielding of the active site [10, 36, 44, 66]. In a recent study, we showed that the bulky and more rigid polyproline sequence used in compound **3** leads to a reduction in packing density when self-assembled on gold, compared with the alkane-based ligand [43]. In the context of our results, this means that ligand rebinding plays a leading role in the observed behavior. These observations certainly emphasize the dynamic nature of the integrin-*c*RGD interactions, providing insights into cellular responses to environmental chemical signaling.

The turnover rates of β3-integrins within FAs established on different *c*RGD-coated surfaces were analyzed using fluorescence recovery after photobleaching (FRAP), in order to understand whether the motile behavior of integrins could be correlated to the affinity of the *c*RGD ligand, and the corresponding stability of the integrin-*c*RGD complex. Single FAs localized at the periphery of the cell were bleached by application of high-intensity laser light, and the recovery of GFP fluorescence measured at different time periods (Figure 6). Cells plated on nanopatterns functionalized with the polyproline-based ligand exhibited the lowest exchange of β3-integrins. Within 350 s, 50% of the integrin fluorescence recovered in the bleached contacts, whereas the exchange on surfaces coated with the Ahx-based ligand was twice as fast. These results compare well with the in vitro αvβ3 integrin binding assays. No significant differences were observed between the Ahx- and the PEG-based ligands, although this discrepancy could be interpreted by considering each pool of integrin measured in the experiment. In FRAP, all integrins, whether bound to the ligand or not, are fluorescently labeled, and within the membrane region probed,

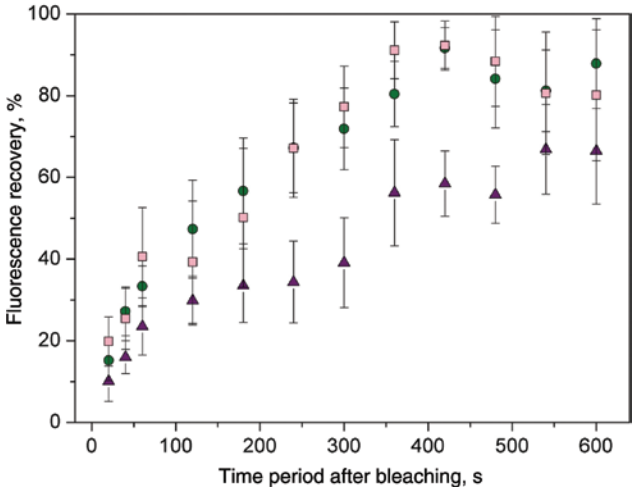


**Figure 6:** Representative FRAP curves for $\beta_3$-GFP integrins. FRAP was performed on FAs localized at the edge of REF52 WT cells transiently expressing $\beta_3$-GFP integrins plated on nanopatterns functionalized with **1** (pink squares), **2** (green circles) and **3** (violet triangles). Values are normalized to the pre-bleaching intensity. Each curve represents fluorescence intensity measurements from several (4–7) cells and three to five individual FAs.

contribute to the signal [67–69]. Furthermore, it could be that the great heterogeneity in lateral mobility could be associated with the experimental conditions. Cells on *c*RGD-coated nanopatterns were evaluated after a 4 h incubation period to match the conditions of the other cell assays, and to minimize the influence of cell-surface interactions provided by the ECM components secreted by the cells, which are thought to be dominant over longer incubation times. Within the 4 h time frame, inherent limitations such as adhesion sliding arise in analyzing FAs within an advancing lamellipodia.

The results obtained for fibroblasts on nanopatterns functionalized with the polyproline-based ligand enable us to infer that β3 integrins display a slower rate of integrin-ligand dissociation, implying longer residence at FAs. A slower diffusion rate can also be associated with higher integrin-ligand affinity [68, 70, 71]. Several studies have shown that increasing the affinity between integrins and the binding domain restricts lateral diffusion. It was recently reported that activation of the high-affinity integrin receptor lymphocyte function-associated antigen 1 (LFA-1) by extracellular $Ca^{2+}$ depletion resulted in reduction of the TS2/4-ATTO520-labeled LFA-1 mobile fraction [71]. In another study, a comparison of lateral diffusion rates between the WT αPS2CβPS and the high-affinity mutant αPS2CβPS409D was made by single-particle tracking, resulting in a decreased mobile fraction and a slower diffusion coefficient for the mutant integrin [68]. These experiments, together with the previous cell adhesion and biochemical experiments, clearly prove that small changes in adhesive chemical cues have a strong influence on the cell adhesion process.

Our most striking finding is that cell adhesive response on *c*RGD-coated substrates strongly depends not only on ligand spatial organization but also on how the ligands are exposed to the integrin extracellular domains. The polyproline sequence, rather than Ahx or PEG-containing spacer, exhibited improved ligand availability at the nanometric scale and as such it stabilized FAs. The extended nature of the polyproline-based dimeric construct is able to display in a more efficient manner the binding moieties leading to higher integrin-binding affinity. This results in higher receptor occupancy and, consequently, provides more suitable nanometric sites for integrin clustering. Consistent with this is the observation that the polyproline sequence yields more stable αvβ3 integrin-*c*RGD complexes characterized by a reduced lateral mobility of integrins, which can be attributed to an effective receptor rebinding. Since integrin clustering is a highly regulated and dynamic process, which involves the recruitment of additional components, it is very likely that the longer residence time of integrin at the binding site favors this process.

Further investigations aiming to identify the number of bound integrins at the binding sites (i.e. AuNPs) with nanometric resolution, as well as essential proteins such as talin or vinculin for integrin activation will be required to achieve a detailed knowledge of the AuNP-binding domain. This challenging endeavor will provide deeper insights into the interplay of physical and biochemical signals governing cell adhesion and influencing cell behavior.

## Conclusions

This article describes the important role of ligand-binding affinity in regulating integrin-mediated cell adhesive responses, by comparing REF52 and MC3T3 cell adhesion behavior on substrates that present *c*(-RGDfX-)-pentapeptides with different ligand-presenting features. For this purpose, we used nanopatterned surfaces containing *c*RGD-biofunctionalized AuNPs surrounded by passivated regions. By varying the chemical nature of the spacer, required for peptide immobilization on the AuNPs, we were able to achieve varying rates of exposure of the ligand to the integrin extracellular domains. We showed that cells plated on nanopatterned surfaces

having polyproline spacers for peptide immobilization could tolerate higher ligand spacings (162 nm) (that means lower ligand density) for FA formation in comparison to cells on the surfaces with *c*RGD immobilized via PEG (110 nm) or Ahx (62 nm) spacers. These results are in partial agreement with our previous studies where we showed that surfaces coated with a *c*RGD peptide bearing Ahx as spacer failed to induce the formation of FAs and stress fibers at an interparticle spacing longer than 70 nm [15, 16]. The current findings indicate that cell adhesive response on *c*RGD-coated substrates strongly depends not only on ligand spatial organization but also on the way the ligands are exposed to the integrin extracellular domains. The hypothesis that the extended nature of the polyproline-based dimeric construct is able to display the binding moieties leading to higher integrin-binding affinity in a more efficient manner, was verified on the cellular level by FRAP measurements. Moreover, the binding affinity assay of αvβ3 integrin and the dissociation rate assay of αvβ3 integrin-*c*RGD complexes were conducted, to confirm the advantageous binding of *c*RGD immobilized ligands via PEG or polyproline spacers. These findings represent an important step towards a deeper understanding of the interactions between cells and their environment, and provide further means to engineer adhesive surfaces to study the mechanisms cells use to sense and respond to different chemical cues.

# Materials and methods

### Chemical synthesis

Peptide synthesis was carried out using TCP resin, following standard Fmoc-strategy [72]. All tested compounds exhibited ≥ 95% purity, as determined by RP-HPLC-(MS). A detailed description of the synthetic procedures was published elsewhere [43]. All synthesized peptides were tested in vitro in a competitive ELISA assay using the natural ligand, vitronectin (Vn), and the soluble human αvβ3 integrin purified receptor [43, 72] (Millipore, Schwalbach/Ts., Germany) (Table 1).

### Biofunctionalized nanopatterns

AuNP quasi-hexagonal patterns were prepared on glass coverslips (Carl Roth, Germany) by means of diblock-copolymer micelle nanolithography (BCML) as previously described [45]. Details concerning the applied diblock copolymers and the casting process are presented in Supporting Information (Table S1, Figures S1 and S2). The area between AuNPs was passivated with mPEG-triethoxysilane (2000) to prevent non-specific adhesion according to a procedure described elsewhere [46]. Each surface was functionalized with the corresponding *c*RGD pentapeptide at a concentration of 25 µM in MilliQ water for 2 h at room temperature. The physisorbed material was removed by thorough rinsing with MilliQ water and PBS. In vitro αvβ3 integrin binding assays and cell adhesion experiments were carried out immediately after this step.

### Cell adhesion experiments

REF52 WT cells were cultured in DMEM medium supplemented with 10% FBS (Invitrogen, Germany) at 37 °C and 5% $CO_2$. For adhesion experiments, cells in culture were rinsed with PBS at 37 °C and adherent cells were removed from the culture surface by treatment with trypsin-EDTA 0.25% (Invitrogen, Germany) for 5 min at 37 °C. Cells were seeded at a density of 150 cells/mm$^2$ on the respective functionalized surfaces in DMEM containing 1% FBS, followed by incubation for 4 h at 37 °C and 5% $CO_2$. Live cell phase contrast microscopy investigation was performed with a 10x/0.25 Ph1 A-Plan objective (Carl Zeiss, Jena, Germany) using an Axiovert 40 CFL microscope (Carl Zeiss, Jena, Germany). Projected cell area was determined manually using ImageJ 1.48 (NIH, http://rsb.info.nih.gov/ij/).

### Immunofluorescence staining

After 4 h on the nanopatterned surfaces, REF52 WT cells were washed with PBS at 37 °C and fixed with 2.5% paraformaldehyde in PBS for 10 min. Cells were then permeabilized with 0.1% Triton X-100 in PBS, blocked with 5% goat serum (Invitrogen, Germany) in PBS for 1 h at room temperature, and incubated with a 1 : 100 dilution of mouse anti-paxillin (Abcam, USA) and with a 1 : 100 dilution of rabbit anti-zyxin (Sigma-Aldrich, Germany) for 1 h at room temperature. Cells were then labeled with a 1 : 100 dilution of goat anti-rabbit Alexa 594-conjugated secondary antibody and with a 1 : 100 dilution of goat anti-mouse Alexa 647-conjugated secondary antibody (Invitrogen, Germany), in 5% goat serum in PBS for 1 h at room temperature. Filamentous actin and nuclei were labeled with Alexa 488-conjugated phalloidin and DAPI (Invitrogen, Germany), respectively. Cells were examined with a 63x/1.25 Oil Ph3 Antiflex Plan-Neofluar objective (Carl Zeiss, Jena, Germany) using an Axiovert 200 epi-fluorescence microscope (Carl Zeiss, Jena, Germany) equipped with a Hamamatsu (model C10600-10B-H) digital CCD camera (Hamamatsu Photonics, Germany). Image processing was achieved with the AxioVision image viewer (Carl Zeiss, Jena, Germany).

### In vitro αvβ3 integrin binding assays

Nanopatterned glass surfaces with a 62 nm interparticle distance and 9 nm particle size, and functionalized with the different *c*RGD pentapeptides, were employed to conduct the integrin binding assays. Two different types of experiments were performed: a) binding affinity of αvβ3 integrin, and b) dissociation rate of αvβ3 integrin-*c*RGD complexes. Binding affinity of αvβ3 integrin towards *c*RGD-nanopatterns was determined in a competitive ELISA-type assay using the soluble pentapeptide *c*(-RGDfK-) and human αvβ3 integrin (Millipore, Schwalbach/Ts., Germany). The amount of αvβ3 integrin adsorbed on the nanopatterns was assessed by immunohistochemistry using primary antibody mouse anti-human CD51/61 (BD Biosciences,

Heidelberg, Germany) and anti-mouse Alexa 488-conjugated secondary antibody (Invitrogen, Germany). A similar procedure was carried out to prepare the samples for determination of the dissociation rate of αvβ3 integrin-*c*RGD complexes. Human integrin αvβ3 was incubated for 24 h in the absence of competition, while fluorescence measurements were conducted in the presence of *c*(-RGDfK-) 100 μM. All experiments were performed at 37 °C, using a microscopy system previously described [73]. Details concerning incubation and washing conditions, as well as measurement conditions and settings, are presented in Supporting Information.

### FRAP measurements

REF52 WT cells were transfected with $\beta_3$-EGFP-integrin plasmid [74] Lipofectamine® 2000 reagent (Invitrogen, Germany), according to the standard manufacturer's protocol. REF52 WT cells expressing β3-GFP integrins were harvested from culture by treatment with trypsin-EDTA 0.25% solution (Gibco Laboratories, Germany). Cells were seeded at a density of 150 cells/mm$^2$ on the respective functionalized surfaces in DMEM containing 1% FBS. Following 4 h of incubation at 37 °C and 5% $CO_2$, nanopatterned glass substrates (62 nm interparticle distance and 9 nm particle size) were mounted on an inverted confocal laser-scanning microscope equipped with an incubation chamber (Leica TCS SP5 X, Leica Mikrosysteme GmbH, Wetzlar, Germany). Confocal images of FA sites were recorded with 5%–6% of the intensity of Ar-Ion gas laser 488 nm line excited via a 63x oil objective (HCX PL APO 63x/1.40-0.60; Leica Mikrosysteme GmbH, Wetzlar, Germany). Five bleach cycles at 50% intensity were used to eliminate the GFP fluorescence at FAs localized at the cell edges. FRAP curves per cell were obtained by considering the fluorescence intensity of three to five individual FA spots. Similar to a previous investigation [74], no newly synthesized $\beta_3$-GFP integrins were detected during the recovery period (up to 10 min).

**Supplemental material:** Experimental details, SEM and TEM characterization of gold nanopatterns, fluorescence micrographs of αvβ3 integrin binding, and supplementary MC3T3 osteoblast adhesion experiments.

**Acknowledgements:** D.P. acknowledges financial support from Max-Planck-Gesellschaft (Max Planck Partner Group Nanoelectronics for Cellular Interfaces). Parts of the research leading to these results have received funding from the European Union Seventh Framework Programme (FP7/2007–2013) under grant agreement Nos. NMP4-LA-2009-229289 NanoII (J.P.S. and B.G.) and NMP3-SL-2009-229294 NanoCARD (J.P.S. and B.G.), as well as from an ERC Advanced Grant under grant agreement No. 294852-SynAd (J.P.S. and B.G.). This work is also part of the MaxSynBio consortium, which is jointly funded by the Federal Ministry of Education and Research of Germany and the Max Planck Society. The authors acknowledge the support of the excellence cluster CellNetworks at the University of Heidelberg. J.P.S. and E.A.C. acknowledge the support from DFG SFB 1129 (P1 and P15). I.P. acknowledges the support of the Alexander von Humboldt Foundation. D.P. is staff researcher of CONICET. J.P.S. is the Weston Visiting Professor at the Weizmann Institute of Science. B.G. is the incumbent of the Erwin Neter Professorial Chair in Cell and Cancer Biology. The Max Planck Society is appreciated for its general support of all aspects of our research. Author's Statement

**Author's statement**

**Conflict of interest:** Authors state no conflict of interest.

**Material and methods:**

**Informed consent:** Informed consent has been obtained from all individuals included in this study.

**Ethical approval:** The research related to human use has been complied with all the relevant national regulations, institutional policies and in accordance the tenets of the Helsinki Declaration, and has been approved by the authors' inistitutional review board or equivalent committee.

## References

1. Geiger B, Spatz JP, Bershadsky AD. Environmental sensing through focal adhesions. Nat Rev Mol Cell Biol. 2009;10:21–33.
2. Hynes RO. Integrins – Versatility, modulation, and signaling in cell-adhesion. Cell 1992;69:11–25.
3. Luo BH, Carman CV, and Springer TA. Structural basis of integrin regulation and signaling. Annu Rev Immunol. 2007;25:619–47.
4. Takagi J, Springer TA. Integrin activation and structural rearrangement. Immunol Rev. 2002;186:141–63.
5. Calderwood DA. Integrin activation. J Cell Sci. 2004;117:657–66.
6. Geiger B, Bershadsky A, Pankov R, Yamada KM. Transmembrane extracellular matrix-cytoskeleton crosstalk. Nat Rev Mol Cell Biol. 2001;2:793–805.
7. Zaidel-Bar R, Itzkovitz S, Ma'ayan A, Iyengar R, Geiger B. Functional atlas of the integrin adhesome. Nat Cell Biol. 2007;9:858–68.
8. Kanchanawong P, Shtengel G, Pasapera AM, Ramko EB, Davidson MW, Hess HF, et al. Nanoscale architecture of integrin-based cell adhesions. Nature 2010;468:58–U262.
9. Yao X, Peng R, Ding J. Cell-material interactions revealed via material techniques of surface patterning. Adv Mater. 2013;25:5257–86.
10. Rodda AE, Meagher L, Nisbet DR, Forsythe JS. Specific control of cell-material interactions: Targeting cell receptors using ligand-functionalized polymer substrates. Prog Polym Sci. 2014;39:1312–47.
11. Balaban NQ, Schwarz US, Riveline D, Goichberg P, Tzur G, Sabanay I, et al. Force and focal adhesion assembly: a close relationship studied using elastic micropatterned substrates. Nat.Cell Biol. 2001;3:466–72.
12. Massia SP, Hubbell JA. An RGD spacing of 440 nm is sufficient for integrin alpha-V-beta-3-mediated fibroblast spreading and 140nm for focal contact and stress fiber formation. J Cell Biol. 1991;114:1089–100.

13. Maheshwari G, Brown G, Lauffenburger DA, Wells A, Griffith LG. Cell adhesion and motility depend on nanoscale RGD clustering. J Cell Sci. 2000;113:1677–86.
14. Irvine DJ, Hue KA, Mayes AM, Griffith LG. Simulations of cell-surface integrin binding to nanoscale-clustered adhesion ligands. Biophys. J. 2002;82:120–32.
15. Arnold M, Cavalcanti-Adam EA, Glass R, Blümmel J, Eck W, Kantlehner M, et al. Activation of integrin function by nanopatterned adhesive interfaces. ChemPhysChem 2004;5:383–8.
16. Cavalcanti-Adam EA, Volberg T, Micoulet A, Kessler H, Geiger B, Spatz JP. Cell spreading and focal adhesion dynamics are regulated by spacing of integrin ligands. Biophys J. 2007;92:2964–74.
17. Schvartzman M, Palma M, Sable J, Abramson J, Hu X, Sheetz MP, et al. Nanolithographic control of the spatial organization of cellular adhesion receptors at the single-molecule level. Nano Let. 2011;11:1306–12.
18. Arnold M, Schwieder M, Blümmel J, Cavalcanti-Adam EA, López-Garcia M, Kessler H, et al. Cell interactions with hierarchically structured nano-patterned adhesive surfaces. Soft Matter 2009;5:72–7.
19. Huang J, Grater SV, Corbellini F, Rinck S, Bock E, Kemkemer R, et al. Impact of order and disorder in RGD nanopatterns on cell adhesion. Nano Lett. 2009;9:1111–6.
20. Deeg JA, Louban I, Aydin D, Selhuber-Unkel C, Kessler H, Spatz JP. Impact of local versus global ligand density on cellular adhesion. Nano Lett. 2011;11:1469–76.
21. Helenius J, Heisenberg CP, Gaub HE, Muller DJ. Single-cell force spectroscopy. J Cell Sci. 2008;121:1785–91.
22. Liu Y, Medda R, Liu Z, Galior K, Yehl K, Spatz JP, et al. Nanoparticle tension probes patterned at the nanoscale: impact of integrin clustering on force transmission. Nano Lett. 2014;14:5539–46.
23. Ruoslahti E. RGD and other recognition sequences for integrins. Annu Rev Cell Dev Biol. 1996;12:697–715.
24. Plow EF, Haas TA, Zhang L, Loftus J, Smith JW. Ligand binding to integrins. J Biol Chem. 2000;275:21785–8.
25. Humphries JD, Byron A, Humphries MJ. Integrin ligands at a glance. J Cell Sci. 2006;119:3901–3.
26. Hynes RO. The extracellular matrix: not just pretty fibrils. Science 2009;326:1216–9.
27. Zamir E, Geiger B. Components of cell-matrix adhesions. J Cell Sci. 2001;114:3577–9.
28. Aumailley M, Gurrath M, Müller G, Calvete J, Timpl R, Kessler H. Arg-Gly-Asp constrained within cyclic pentapeptides – strong and selective inhibitors of cell-adhesion to vitronectin and laminin fragment-P1. FEBS Lett. 1991;291:50–4.
29. Haubner R, Finsinger D, Kessler H. Stereoisomeric peptide libraries and peptidomimetics for designing selective inhibitors of the alpha(V)beta(3) integrin for a new cancer therapy. Angew Chem Int Edit. 1997;36:1375–89.
30. Mas-Moruno C, Rechenmacher F, Kessler H. Cilengitide: the first anti-angiogenic small molecule drug candidate design, synthesis and clinical evaluation. Anticancer Agents Med Chem. 2010;10:753–68.
31. Chatterjee J, Rechenmacher F, Kessler H. N-methylation of peptides and proteins: an important element for modulating biological functions. Angew Chem Int Edit. 2013;52:254–69.
32. Temming K, Schiffelers RM, Molema G, Kok RJ. RGD-based strategies for selective delivery of therapeutics and imaging agents to the tumour vasculature. Drug Resist Updates 2005;8:381–402.
33. Kiessling LL, Gestwicki JE, Strong LE. Synthetic multivalent ligands as probes of signal transduction. Angew Chem Int Edit. 2006;45:2348–68.
34. Lössner D, Kessler H, Thumshirn G, Dahmen C, Wiltschi B, Tanaka M, et al. Binding of small mono- and oligomeric integrin ligands to membrane-embedded integrins monitored by surface plasmon-enhanced fluorescence spectroscopy. Anal Chem. 2006;78:4524–33.
35. Wängler C, Maschauer S, Prante O, Schäfer M, Schirrmacher R, Bartenstein P, et al. Multimerization of cRGD peptides by click chemistry: synthetic strategies, chemical limitations, and influence on biological properties. Chembiochem 2010;11:2168–81.
36. Hersel U, Dahmen C, Kessler H. RGD modified polymers: biomaterials for stimulated cell adhesion and beyond. Biomaterials 2003;24:4385–415.
37. Salinas CN, Anseth KS. The influence of the RGD peptide motif and its contextual presentation in PEG gels on human mesenchymal stem cell viability. J Tissue Eng Regen Med. 2008;2:296–304.
38. Kantlehner M, Finsinger D, Meyer J, Schaffner P, Jonczyk A, Diefenbach B, et al. Selective RGD-mediated adhesion of osteoblasts at surfaces of implants. Angew Chem Int Edit. 1999;38:560–2.
39. Mas-Moruno C, Fraioli R, Albericio F, Manero JM, Gil FJ. Novel peptide-based platform for the dual presentation of biologically active peptide motifs on biomaterials. ACS Appl Mater Inter. 2014;6:6525–36.
40. Kalinina S, Gliemann H, López-García M, Petershans A, Auernheimer J, Schimmel T, et al. Isothiocyanate-functionalized RGD peptides for tailoring cell-adhesive surface patterns. Biomaterials 2008;29:3004–13.
41. Kilian KA, Mrksich M. Directing stem cell fate by controlling the affinity and density of ligand-receptor interactions at the biomaterials interface. Angew Chem Int Edit. 2012;51:4891–5.
42. Petrie TA, Capadona JR, Reyes CD, García AJ. Integrin specificity and enhanced cellular activities associated with surfaces presenting a recombinant fibronectin fragment compared to RGD supports. Biomaterials 2006;27:5459–70.
43. Pallarola D, Bochen A, Boehm H, Rechenmacher F, Sobahi TR, Spatz JP, et al. Interface immobilization chemistry of cRGD-based peptides regulates integrin mediated cell adhesion. Adv Funct Mater. 2014;24:943–56.
44. Kingshott P, Thissen H, Griesser HJ. Effects of cloud-point grafting, chain length, and density of PEG layers on competitive adsorption of ocular proteins. Biomaterials 2002;23:2043–56.
45. Glass R, Möller M, Spatz JP. Block copolymer micelle nanolithography. Nanotechnology 2003;14:1153–60.
46. Blümmel J, Perschmann N, Aydin D, Drinjakovic J, Surrey T, Lopez-Garcia M, et al. Protein repellent properties of covalently attached PEG coatings on nanostructured SiO2-based interfaces. Biomaterials 2007;28:4739–47.
47. Xiong JP, Stehle T, Zhang R, Joachimiak A, Frech M, Goodman SL, et al. Crystal structure of the extracellular segment of integrin alpha V beta 3 in complex with an Arg-Gly-Asp ligand. Science 2002;296:151–5.
48. Curtis A, Riehle M. Tissue engineering: the biophysical background. Phys Med Biol. 2001;46, R47–65.
49. Dalby MJ, Riehle MO, Johnstone H, Affrossman S, Curtis AS. In vitro reaction of endothelial cells to polymer demixed nanotopography. Biomaterials 2002;23:2945–2954.

50. Vogel V, Sheetz M. Local force and geometry sensing regulate cell functions. Nat Rev Mol Cell Biol. 2006;7:265–75.
51. Spatz JP, Geiger B. Molecular engineering of cellular environments: Cell adhesion to nano-digital surfaces. In: Wang YL, Discher DE, editors. Cell Mechanics, 2007;89–111.
52. Platzman I, Muth CA, Lee-Thedieck C, Pallarola D, Atanasova R, Louban I, et al. Surface properties of nanostructured bio-active interfaces: impacts of surface stiffness and topography on cell-surface interactions. RSC Adv. 2013;3:13293–303.
53. Mammen M, Choi SK, Whitesides GM. Polyvalent interactions in biological systems: Implications for design and use of multivalent ligands and inhibitors. Angew Chem Int. Edit. 1998;37:2755–94.
54. Kiessling LL, Gestwicki JE, Strong LE. Synthetic multivalent ligands in the exploration of cell-surface interactions. Curr Opin Chem Biol. 2000;4:696–703.
55. Schwarz US, Alon R. L-selectin-mediated leukocyte tethering in shear flow is controlled by multiple contacts and cytoskeletal anchorage facilitating fast rebinding events. Proc Nat Acad Sci USA 2004;101:6940–5.
56. Dijkgraaf I, Kruijtzer JA, Liu S, Soede AC, Oyen WJ, Corstens FH, et al. Improved targeting of the alpha(v)beta(3) integrin by multimerisation of RGD peptides. Eur J Nucl Med Mol Imaging 2007;34:267–73.
57. Schiller HB, Fassler R. Mechanosensitivity and compositional dynamics of cell-matrix adhesions. EMBO Rep. 2013;14:509–19.
58. Choi CK, Zareno J, Digman MA, Gratton E, Horwitz AR. Cross-correlated fluctuation analysis reveals phosphorylation-regulated paxillin-FAK complexes in nascent adhesions. Biophys J. 2011;100:583–92.
59. Hirata H, Tatsumi H, Sokabe M. Mechanical forces facilitate actin polymerization at focal adhesions in a zyxin-dependent manner. J Cell Sci. 2008;121:2795–804.
60. Takada Y, Ye X, Simon S. The integrins. Genome Biol. 2007;8:215.
61. Kato M, Mrksich M. Using model substrates to study the dependence of focal adhesion formation on the affinity of integrin-ligand complexes. Biochemistry 2004;43:2699–707.
62. Zhao T, Li Y, Dinner AR. How focal adhesion size depends on integrin affinity. Langmuir 2009;25:1540–6.
63. Bochen A, Marelli UK, Otto E, Pallarola D, Mas-Moruno C, Di Leva FS, et al. Biselectivity of IsoDGR peptides for fibronectin binding integrin subtypes alpha5beta1 and alphavbeta6: conformational control through flanking amino acids. J Med Chem. 2013;56:1509–19.
64. Pérez-Luna VH, O'Brien MJ, Opperman KA, Hampton PD, López GP, Klumb LA, et al. Molecular recognition between genetically engineered streptavidin and surface-bound biotin. J Am Chem Soc. 1999;121:6469–78.
65. Sato Y, Yoshioka K, Murakami T, Yoshimoto S, Niwa O. Design of biomolecular interface for detecting carbohydrate and lectin weak interactions. Langmuir 2012;28:1846–51.
66. Beer JH, Springer KT, and Coller BS. Immobilized Arg-Gly-Asp (RGD) peptides of varying lengths as structural probes of the platelet glycoprotein IIb/IIIa receptor. Blood 1992;79:117–28.
67. Georgiou G, Bahra SS, Mackie AR, Wolfe CA, O'Shea P, Ladha S, et al. Measurement of the lateral diffusion of human MHC class I molecules on HeLa cells by fluorescence recovery after photobleaching using a phycoerythrin probe. Biophys J. 2002;82:1828–34.
68. Mainali D, Smith EA. The effect of ligand affinity on integrins' lateral diffusion in cultured cells. Eur Biophys J Biophy. 2013;42:281–90.
69. Levental I, Lingwood D, Grzybek M, Coskun U, Simons K. Single particle tracking with sterol modulation reveals the cholesterol-mediated diffusion properties of integrin receptors. Phys Biol. 2014;11:066001.
70. Levental I, Lingwood D, Grzybek M, Coskun U, Simons K. Palmitoylation regulates raft affinity for the majority of integral raft proteins. Proc Nat Acad Sci USA 2010;107:22050–4.
71. Bakker GJ, Eich C, Torreno-Pina JA, Diez-Ahedo R, Perez-Samper G, van Zanten TS, et al. Lateral mobility of individual integrin nanoclusters orchestrates the onset for leukocyte adhesion. Proc Nat Acad Sci USA 2012;109:4869–74.
72. Fields GB, Noble RL. Solid phase peptide synthesis utilizing 9-fluorenylmethoxycarbonyl amino acids. Int J Pept Protein Res. 1990;35:161–214.
73. Deeg J, Axmann M, Matic J, Liapis A, Depoil D, Afrose J, et al. T cell activation is determined by the number of presented antigens. Nano Lett. 2013;13:5619–26.
74. Ballestrem C, Hinz B, Imhof BA, Wehrle-Haller B. Marching at the front and dragging behind: Differential αvβ3-integrin turnover regulates focal adhesion behavior. J Cell Biol. 2001;155:1319–32.

**Supplemental Material:** The online version of this article (DOI: 10.1515/bnm-2016-0014) offers supplementary material, available to authorized users.